Journal of Materials Chemistry B

ROYAL SOCIETY OF CHEMISTRY

PAPER

View Article Online
View Journal | View Issue

Cite this: J. Mater. Chem. B, 2025, 13, 2317

Metal–organic frameworks as anchors for giant unilamellar vesicle immobilization†

Aroosha Faheem, [a] Mason C. Lawrence, [a] Gazi A. Bushra, [a] M.-Vicki Meli [b] and Barry A. Blight *[a]

Received 12th September 2024,
Accepted 15th January 2025

DOI: 10.1039/d4tb02055c

rsc.li/materials-b

Giant unilamellar vesicles (GUVs) are ideal for studying cellular mechanisms due to their cell-mimicking morphology and size. The formation, stability, and immobilization of these vesicles are crucial for drug delivery and bioimaging studies. Separately, metal–organic frameworks (MOFs) are actively researched owing to their unique and varied properties, yet little is known about the interaction between MOFs and phospholipids. This study investigates the influence of the metal–phosphate interface on the formation, size distribution, and stability of GUVs with different lipid compositions. GUVs were electroformed in the presence of a series of MOFs. The results show Al, Zn, Cu, Fe, Zr, and Ca metal centers of MOFs can coordinate to phospholipids on the surface of GUVs, leading to the formation of functional GUV@MOF constructs, with stablilities over 12 hours. Macroscopically, society has seen biology (people, plants, microbes) interacting with inorganic materials regularly. We now explore how microscopic biological models behave in the presence of inorganic constructs. This research opens new avenues for advanced biomedical applications interacting tailored frameworks with liposomes.

Introduction

Metal–organic frameworks (MOFs) are known for their highly ordered structures and exceptional versatility and have been investigated as key materials in a wide array of biomedical applications.[1–5] Their unique properties featuring tuneable pore sizes, high surface areas, and inherent stability make MOFs ideal candidates for innovative solutions in this area.[1] MOFs have been previously used as carriers for delivery of DNA and proteins, where their tuneable pore size allows for high loading, while their inherent stability ensures that the payload is released in a controlled manner.[6] MOFs have been used as high sensitivity biosensors, with high surface area playing a key role in providing extensive binding sites for the immobilization of analytes.[7,8] Concomitantly, giant unilamellar vesicles (GUVs) are very popular cell models.[9] These sizable liposomes are important for studying membrane biophysics, interactions between membrane molecules, anion transport, and drug delivery for advanced therapeutics.[10] Studies have reported MOF liposome assemblies that include but are not limited to the use of lipid-coated MOF nanoparticles,[11,12] liposomes encapsulated in MOFs,[13,14] MOFs embedded in lipid membranes of liposomes,[15] and the use of MOFs with lipid functionalized surfaces.[16]

In recent literature, water-stable functionalized Hf and Zr MOFs embedded within liposome bilayer demonstrated the potential of sustainable energy production by facilitating photocatalytic splitting of water into H_2 and O_2 by sunlight irradiation. The lipid membrane efficiently separated the oxidative and reductive components of the system for charge separation.[15] The stabilization of integrated MOFs within the liposome membrane may be largely dependent on the interaction between the embedded framework and the phosphate groups of the membrane that likely influence the photocatalytic water splitting performance of MOFs. In another study, MIL-100(Fe) MOF nanoparticles encapsulated in 1,2-dioleoyl-*sn*-glycero-3-phosphocholine (DOPC) liposomes induced cell death by releasing high amount of Fe^{3+} ions in the cells depending upon the acidification of extracellular pH. The phospholipid coating facilitated the uptake of MOFs by endocytosis which resulted in an effective strategy against cancer cells.[17] Thus, despite growing interest in biomedical applications of MOFs, there currently is a lack of understanding of the chemical interaction of the MOFs with phospholipids. Specifically, the binding of MOFs to phospholipids, a key component of cell membranes, is not well studied. This knowledge gap hinders the development of intricate MOF-based hybrid systems that can mimic nature's machinery and effectively intermingle with and target specific cells.

[a] Department of Chemistry, University of New Brunswick, Fredericton, New Brunswick, Canada. E-mail: b.blight@unb.ca
[b] Department of Chemistry and Biochemistry, Mount Allison University, Sackville, New Brunswick, Canada

† Electronic supplementary information (ESI) available. See DOI: https://doi.org/10.1039/d4tb02055c

The primary method to observe GUVs is by using microscopy due to the large size of vesicles (1–100 μm). The protocols for imaging liposomes, however, are limited as the vesicles freely move after harvesting in the solution, hindering the analysis and imaging, particularly confocal *z*-stacking. Typically, a sucrose/glucose density gradient is used for the gravity-based sedimentation of liposomes in the imaging well, while maintaining freedom of lateral movement.[18] Other work in the area extends the approaches by using biotin–streptavidin interaction, DNA immobilization, magnetic, electric, and acoustic field trapping.[19–23] Strategies involving the covalent anchoring allows for detailed observation of GUVs with an increased risk of membrane modification/deformation and are costly. GUVs have been held in hydrogels and agarose gel to investigate single liposomal membrane properties without any adverse effect on vesicle stability.[24,25] This limits the use of inverted microscopes, and the hydrogel constituents can incorporate the membrane or lumen of the GUVs which may not be desired for the study.[26] Alternatively, GUVs can be physically trapped in microfluidic channels or chambers/wells for imaging, holding a random population of GUVs. The vesicles compress as they make their way into the channels, hence microfluidic setups can influence membrane elasticity, potentially altering their mechanical properties and making them poor comparisons to physiological cell models.[27,28] Although these methods offer imaging possibilities, most of them are impractical for implementation.

Contrary to the traditional GUV immobilizing approaches, an innovative and inexpensive approach to address this challenge is the immobilization of GUVs with MOFs. In 2021, we reported the use of zirconium MOFs to anchor GUVs on a timescale of minutes to hours owing to the affinity of zirconium ions to strongly bind phosphate groups in phospholipid membranes.[29] We herein expand on this work, exploring the immobilization of vesicles with different lipids compositions to various micron-sized MOFs, including MIL-53(Al) MIL-100(Al), MOF-177, Cu BDC, HKUST-1, MIL-53(Fe), MIL-100(Fe), UiO-66, MOF-808, Ca BDC and MgMOF-74. These MOFs were chosen for their varied chemical compositions and structural characteristics, which provide a basis for the binding of metal centres or ligands with lipid bilayers. We used lipid mixtures with saturated (1,2-dipalmitoyl-*sn-glycero*-3-phosphocholine; DPPC), unsaturated (1,2-dioleoyl-*sn-glycero*-3-phosphocholine; POPC and DOPC) and negatively charged (1-palmitoyl-2-oleoyl-*sn-glycero*-3-phospho-(1′-*rac-glycerol*); POPG) lipids in combination with cholesterol (Chol) in this study. The development of inorganic compounds that can interact with biological membranes is a crucial interface for the application of materials science in life sciences. In this study, we aim to bridge the gap by evaluating the phospholipid anchoring capacity of a diverse set of MOFs, examining their influence on GUV formation, size distribution, frequency of immobilization, and stability.

Results and discussion

To elucidate the MOF–phospholipid interactions we developed a series of experiments to determine which structural features of the MOFs interact with the phospholipids. The topology and structure of MOFs is determined by two features, the Lewis acidic metal centres and the organic bridging ligands containing multiple Lewis basic sites. Both metal centre and ligands were varied in producing a series of 11 known metal organic–frameworks to investigate how these features impact MOF–GUV interactions.

We synthesized aluminium, copper, iron, zirconium, and calcium based MOFs with a benzene-1,4-dicarboxylate ligand; aluminium, copper, iron, and zirconium based MOFs with benzene-1,3,5-tricarboxylic acid; zinc with 1,3,5-tri(4-carboxyphenyl)benzene; magnesium with 2,5-dihydroxy-1,4-benzenedicarboxylic acid ligands. Fig. 1 illustrates the anchoring of MOF particles to GUVs during the swelling of POPC : POPG : Chol lipid layers, demonstrating the interaction between the MOFs and GUV membrane. Thus, by varying the metal centre and ligand, we aimed to identify the key factors governing MOF–GUV interactions.

GUVs are formed by hydrating the lipid films, the lipid molecules due to their amphipathic nature self-assemble upon addition of water such that the hydrophobic tails are shielded, and hydrophilic heads extend outside forming the vesicle. In 1986, Angelova and Dimitrov improved the protocol by applying an alternating current (AC) electric field during the swelling process which significantly improved vesicle yield, monodispersity, and unilamellarity. The electroformation protocol is now well established as researchers have worked around the application of different AC frequencies, amplitudes, temperature parameters, and electrodes (ITO/Pt) to get GUVs in required conditions.

GUVs were electroformed on indium-tin oxide (ITO) conductive electrodes in HEPES buffer (pH 7.4) containing sucrose and a small amount of MOF sample, and resuspended them in a glucose containing buffer following a literature procedure.[29] This facilitates vesicle imaging, as the encapsulated sucrose solution in the GUV is more dense than the glucose solution

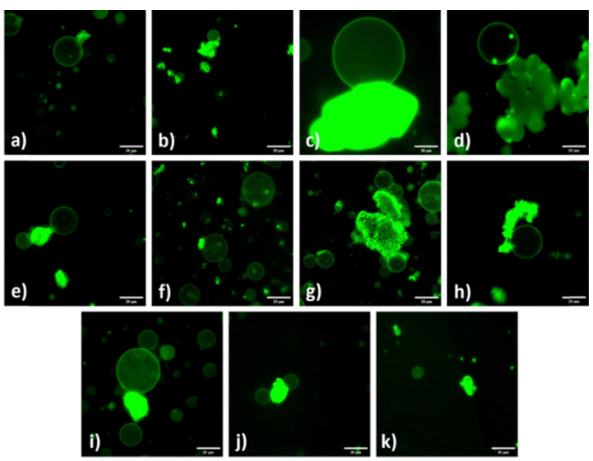

Fig. 1 Fluorescence images of POPC : POPG : Chol (4 : 1 : 1) GUVs immobilized by MOF particles (a) GUV/MIL-53(Al) (b) GUV/MIL-100(Al) (c) GUV/MOF-177 (d) GUV/CuBDC (e) GUV/HKUST-1/GUV (f) GUVs/MIL-53(Fe) (g) GUVs/MIL-100(Fe) (h) GUV/UiO-66 (i) GUVs/MOF-808 (j) GUVs/CaBDC (k) MgMOF-74. Scale bars represent 20 μm.

surrounding the vesicle causing them to settle near the bottom of the imaging wells. Yet, the electroformed GUVs sedimented this way are still mobile.

Zr-BTDZ MOF and MOF-808, as previously reported, have the ability to immobilize GUVs[29] and we hypothesize other MOFs also have the same capability. The lipid mixtures used in this study are POPC : POPG : Chol 4 : 1 : 1 (2 mg ml^{-1}), POPC : Chol 7 : 3 (2 mg ml^{-1}), and DOPC : DPPC : Chol 1 : 1 : 20 mol% (2 mg ml^{-1}). Each lipid mixture has an additional TopFluor Chol 0.1 mol% of the concentration of cholesterol for imaging (see ESI† for detailed GUV formation procedure).

It is important to study a model vesicle system comprised of a combination of fully saturated lipid, unsaturated lipid, and cholesterol to mimic cellular lipid rafts. However, saturated lipids with higher phase transition temperatures (T_m) remain in the ordered gel phase making liposome formation challenging. Therefore, we used saturated lipid DPPC (T_m 41 °C) in combination with unsaturated lipid DOPC (T_m −17 °C) which has better miscibility in the ordered phase yielding a more stable and organized membrane structure. In addition, we also investigated a negatively charged lipid, POPG, that is traditionally used in combination with zwitterionic lipids such as POPC/POPE/DSPC in GUVs. Due to the residing negative charge, it has been shown to help bind proteins to the surface of GUVs.[30] A relatively low concentration of POPG is required for electroformation of GUVs in ionic solutions as it provides lamellar repulsion that facilitates the peeling of lipid layers during GUV formation. At physiological pH, both POPC and POPG have a zero-lipid intrinsic curvature (the tendency to form curved structures), where POPC remains neutral and POPG carries a negative charge.[31] Hence, based on the metal–phosphate electrostatic interaction we sought to examine if cationic metal centres in MOFs acting as Lewis acids bind to the phosphate groups of lipids and if the interaction is more prominent in a negatively charged lipid mixture compared to a neutral control POPC : Chol mix.

To determine if MOF–GUV anchoring was accomplished GUVs were imaged using Echo Discover Revolve Fluorescent microscope in the FITC channel immediately after electroformation. If MOF–GUV anchoring was successful, the GUV and MOF are stationary in the examined solution on the glass slide; if the GUV anchoring is unsuccessful, the GUVs tend to be free flowing in solution as observed in our control experiments.

Vesicle yield and immobilization

Notable differences in the sizes of resulting GUVs were recorded. To identify the influence of MOF particles on the size of GUVs, the area of the vesicles was measured using ImageJ software from three representative images per MOF sample (Fig. 2(b)). GUVs smaller than 5 μm and larger than 80 μm in diameter were not included in the analysis. The disparity in the yield of GUVs favoured or suppressed by MOFs using respective lipid mixtures is shown in Fig. 2(a). The control experiments in which no MOF particles were included, consistently yielded a moderate number of GUVs across all lipid compositions, serving as a baseline for comparison. The POPC : POPG : Chol lipid composition showed

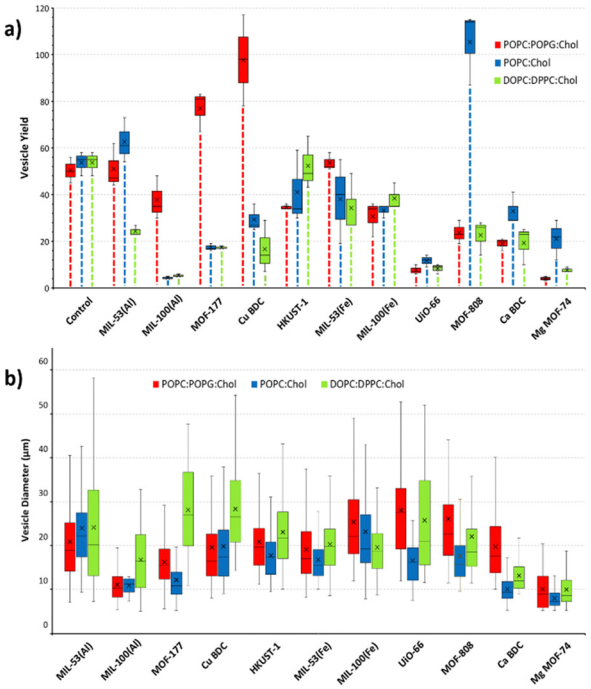

Fig. 2 Trends in GUVs formed with POPC : POPG : Chol, POPC : Chol and DOPC : DPPC : Chol lipid mixtures (a) GUV yield in presence of respective MOFs quantified from three images from different experiments per lipid mixture (b) vesicle diameter in presence of respective MOFs. Each box and whisker plot shows the median (centre line), interquartile range (box), data range (whiskers), and mean value (indicated by the cross).

84% of GUV size distribution with in 20–40 μm range but for POPC : Chol and DOPC : DPPC : Chol lipid mixtures the majority of GUV sizes lies between 10–30 μm resulting in frequency distribution of 89% and 70%, respectively. Nonetheless, the vesicle yield trends, and frequency size distribution (Fig. 3) varied significantly when MOF particles were introduced during electroformation, showcasing the influence of MOF properties on GUV formation. The differences are discussed in the respective sections of each MOF. In addition to two-component adducts (GUV@MOF), GUVs bound to multiple sites on a MOF particle and a single MOF particle binding two distinct GUVs were also observed with HKUST-1, MOF-808, MIL-100(Fe).

Aluminium MOFs with phospholipids

Aluminium MOFs have not been studied for drug delivery or interactions with phospholipids up to this point. To get insights on the anchoring of these frameworks with GUV membrane we referred to the literature reporting absorption of phosphates with Al fumarate MOF, MIL-53(Al), and MIL-100(Al) MOFs. This study showed that by varying the pH of the solution, both electrostatic interactions and ligand exchange mechanisms between phosphate anions and Al^{3+} nodes were observed, and that maximum phosphate absorption occurs at a neutral pH, where electrostatic interactions were responsible for phosphate absorption.[32] Subsequently, in our experiments (conducted at pH 7.4), the MOF GUV anchoring observed is likely driven by electrostatic or weakly coordinating

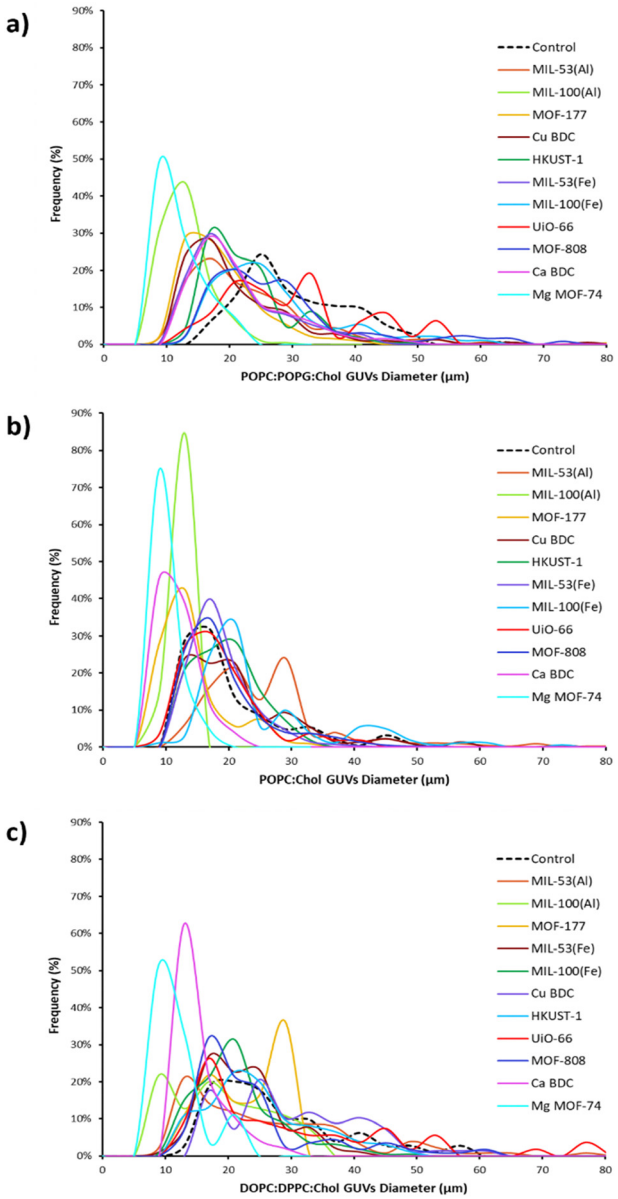

Fig. 3 Size distribution of GUVs based on their lipid composition is presence of MOFs (a) with POPC : POPG : Chol (b) with POPC : Chol (c) with DOPC : DPPC : Chol. The plots show that the frequency (%) of GUVs sizes produced in respective lipid mixtures varies with different MOFs. The black dotted line indicates the GUVs formed with these lipid mixtures in the absence of MOFs, serving as a reference.

interactions between the electropositive aluminium centre and the electronegative lipid layer. GUVs were produced in the presence and immobilized by MIL-53 using each of the lipid compositions and MIL-100(Al) using negatively charged lipid mix, respectively (Fig. S3–S5, ESI†). MIL-53(Al) displayed not only favourable GUV growth with all lipid compositions (Fig. S6a, ESI†), but giant GUVs up to 100–250 μm were produced in POPC : Chol lipid mixture (Fig. S21, ESI†). MIL-53(Al) particles, being smaller than MIL-100(Al), offer a reduced surface area for interaction, which can impact both GUV formation and anchoring efficiency. Smaller MOFs seems less effective in interacting with the lipid layers during electroformation, resulting in fewer GUVs or smaller vesicle sizes compared to larger MOFs like MIL-100(Al). Thus, there were moderate instances of GUV immobilization due to small size of MOF particles. Conversely, we observed both a drop in the number of GUVs produced and reduction in vesicle diameter with MIL-100(Al) (Fig. S6b, ESI†). GUV anchoring was observed with a negatively charged lipid mixture and DOPC : DPPC : Chol lipid (Fig. S3b and S5b, ESI†). GUVs formed in the presence of this framework with POPC : Chol did not demonstrate immobilization (Fig. S4b, ESI†) and showed the smallest size distribution among all MOFs with vesicle diameters ranging from 7–13 μm (Fig. 2(b)). The difference in ligand topology (terephthalic acid, bidentate *vs.* trimesic acid, tridentate) results in important structural changes that may have influenced GUV production and immobilization. Supplementary Videos SV1 and SV2 (ESI†) demonstrate the POPC : POPG : Chol GUV@MOF with MIL-53(Al) and MIL-100(Al), respectively.

Iron MOFs with phospholipids

Iron MOFs, like aluminium frameworks, are excellent phosphate absorbents and are good candidates for water treatment. Concerning the binding mechanisms of phosphates to iron MOFs, Vargas *et al.* reported ligand exchange with non-structural and structural (carboxyl) OH^- groups in iron oxide centres. As such, MIL-53(Fe) and MIL-100(Fe) both provides potential binding sites for efficient phosphate absorption.[33] Another mechanism for phosphate retention was demonstrated using MIL-100(Fe). The authors suggested that anion absorption was observed because the resulting –COO–Fe^{3+} cluster is Lewis acidic and attracts the electronegative PO_4^{3-} ions. In the case of $H_2PO_4^-$ binding, electrostatic interactions as well as anion metal coordination were observed.[34] In this study, the immobilization of GUVs to iron MOFs is observed (Supplementary Videos SV3 and SV4, ESI†), with association behaviour similar to those seen in the aluminium MOFs. A good yield of GUVs was formed in presence of iron MOFs with both ligands (MIL-53 and MIL-100 (Fe); Fig. 2(a)). Here, the large number of GUVs produced suggests these MOFs do not hinder vesicle formation. With MIL-53(Fe) we observed small MOF particles as well as MOF clusters that impacted GUV anchoring differently. MIL-53(Fe) clusters immobilized GUVs for extended time duration (Fig. S16a, ESI†). Whereas there were limited observed instances of GUV anchoring with individual MOF particles. The GUVs with smaller MIL-53(Fe) particles were actively mobile during the imaging process, (Fig. S16b and c, ESI†) and showed some reversible interactions with MIL-53(Fe) particles for a few seconds as they were passing by. Such fluidity in the vesicle indicates that membrane rigidity and stability are compromised. Alternatively, multiple GUV@MOFs with MIL-100(Fe) particles were observed and remained stable during imaging (Fig. S17, ESI†). The larger size and extended metal node structures of MIL-100(Fe) particles provided more robust anchoring, with stable GUV immobilization observed during imaging and over extended periods. This behaviour suggests that the particle size and aggregation state of MIL-53(Fe)

influence its anchoring ability. The GUV diameters were slightly larger and had broader size distribution with all lipid mixtures compared to MIL-53(Fe) (Fig. 2(b) and Fig. S9, ESI†). We see a similar trend in GUV yield for both iron MOFs as reported with aluminium frameworks indicating large number of vesicles being produced with dicarboxylic acid *versus* tricarboxylic acid ligands (Fig. 2(a)). See Supplementary Video SV11 (ESI†) for confocal *z*-stack of a GUV immobilized by MIL-100(Fe).

Copper MOFs with phospholipids

The interaction of copper MOFs with phospholipids is not widely studied. Yet, Lee *et al.* reported a copper MOF immersed in phosphate-buffered saline formed a flower-like deposition on the surface of MOF due to the reaction of copper cations with phosphate anions. This copper–phosphate coating prevented the release of Cu^{2+} ions to a great extent making these MOFs a stable candidate for aqueous physiological applications.[35] Our results showed many GUV@MOFs in the imaging wells with both CuBDC and HKUST-1 when tested with each lipid mixture, suggesting affinity of copper nodes for phospho-lipids (Fig. S3–S5, ESI†). Supplementary Videos SV5 and SV6 (ESI†) provides a visual representation of POPC : POPG : Chol GUV@MOF with CuBDC and HKUST-1, the Video SV12 (ESI†) shows a confocal *z*-stack of a GUV immobilized by HKUST-1. To visualize further, we employed SEM and dry-stage atomic force microscopy (AFM) analysis for GUV@HKUST-1. Fig. 4(a) shows a collapsed GUV attached to the MOF particle under SEM (Fig. S36, ESI† illustrates the corresponding EDS analysis). The deformation in the vesicle shape is due to the sample preparation protocol, details mentioned in the ESI.† Likewise, AFM analysis (Fig. S38, ESI†) also provides evidence of physical interaction between the vesicle membrane and the MOF surface. The procedure and imaging details are included in the ESI.† The mean vesicle diameter with CuBDC was within 10 μm range for all lipid mixtures and relatively close (18–23 μm range) with HKUST-1 (Fig. S8, ESI†). The POPC : Chol lipid mix yielded a vesicle size similar to POPC : POPG : Chol lipid mix while largest diameters observed in GUVs formed from DOPC : DPPC : Chol lipid mix (Fig. 2(b)). The number of GUVs formed with negatively charged lipid composition in presence of CuBDC was significantly higher than all other MOFs with this lipid composition. Alternatively, the vesicle yield with DOPC : DPPC : Chol mixture in CuBDC was lower compared to other MOFs and almost half of the GUVs produced with HKUST-1 (Fig. 2(a)). With CuBDC, we also recorded relatively broad size frequency (%) distribution, and GUVs up to 82 μm diameters were seen (Fig. 3(c) and Fig. S8a, ESI†).

Zirconium MOFs with phospholipids

As discussed previously, zirconium frameworks have been extensively used in drug delivery studies,[36,37] for anchoring biomolecules such as enzymes[38] and phospholipid vesicles.[29] In previous studies, a strong attraction of zirconium MOFs for phosphoric acid groups was observed in Zr–O nodes in UiO-66 nanoparticles. The nodes participated in Zr–O–P bond formation to capture phosphorous species.[39] Similar cationic interaction was observed with zirconium ions and oxygens of

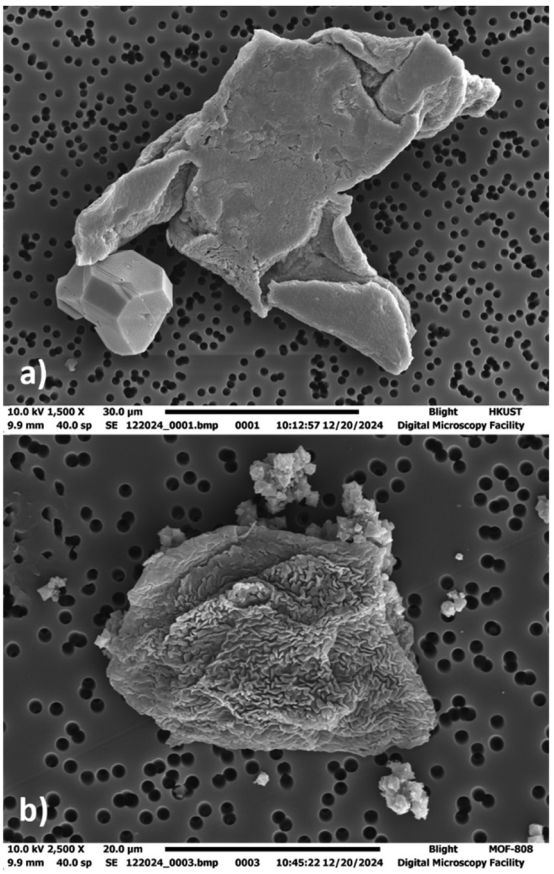

Fig. 4 SEM images of deflated GUVs under OsO_4 vesicle preservation (a) GUV@HKUST-1 (b) GUV@MOF-808 (b). See ESI† (S36, S37) for EDS analysis.

the phospholipid headgroup in the GUV membrane that ensures stable anchoring of the lipid bilayer.[29] We investigated two zirconium MOFs that share common chemistry but significantly different topology due to varying ligands: UiO-66 (made with linear disposed terephthalic acid) has relatively smaller particles and MOF-808 with trigonally disposed benzene tricarboxylate as a ligand. We have previously demonstrated GUV immobilization with MOF-808 and fluorescent Zr-BTDZ.[29] We extend our understanding by exploring its interaction with the DOPC : DPPC : Chol lipid mixture and investigating GUV@MOF viability over 12 hours, insights that had not been reported. The results show GUVs readily immobilized with both UiO-66 and MOF-808 with all lipid mixtures (Fig. S3–S5 and Supplementary Videos SV7, SV8, ESI† showcase GUV@MOF anchoring). To further illustrate MOF–GUV interface, refer to Supplementary Videos SV13 and SV14 (ESI†) showing confocal *z*-stacks of GUV@UiO-66 and GUV@MOF-808. The SEM analysis of GUV@-MOF-808 (Fig. 4(b)) revealed a deflated GUV attached to MOF-808 crystals, highlighting that GUVs remain immobilized on crystalline MOF particles even after intensive sample preparation (Fig. 4(b)). Additionally, EDS spectra provided in the ESI† (Fig. S37) confirms the presence of Zr peaks, further validating the MOF particles. The trend in the vesicle diameter was the same for both zirconium MOFs where the POPC : Chol mix

showed narrow GUV size distribution producing smaller GUVs (mean diameter 17 μm with UiO-66 and 18 μm with MOF-808; Fig. 3(b) and Fig. S10, ESI†). In terms of GUV yield, a high number of GUVs were formed in presence of MOF-808 compared to UiO-66 for all lipid compositions (Fig. 2(a)). We anticipate this is because UiO-66 particles are smaller and more dispersed in the electroformation solution and would lead to more interactions with the phospholipid layers during GUV electroformation. Our study also revealed that the zirconium MOFs with benzene tricarboxylate ligand (*i.e.* MOF-808) demonstrated GUV binding seen at multiple sites in the imaging well and notable increase in GUV yield, compared to dicarboxylate MOF UiO-66.

Biocompatible MOFs with phospholipids

In addition to aluminium, iron, copper, and zirconium-based MOFs, we evaluated three biocompatible MOFs (MOF-177 (zinc), CaBDC (calcium), and MgMOF-74 (magnesium)) to investigate their GUV immobilization potential. Zinc MOFs have been extensively studied in biomedical applications due to their compatibility and biodegradability with biomolecules.[40] The zinc based MOF-177 showed viable GUVs being produced and anchored in all three lipid mixtures (Fig. S3c, S4c, S5c, ESI†). The number of GUVs produced with a negatively charged lipid mixture was two-fold more than the other two lipid compositions (Fig. 2(a)), see Supplementary Video SV9 (ESI†) for GUV@MOF adduct. The vesicle size with DOPC : DPPC : Chol lipid was relatively large (mean diameter 28 μm) compared to POPC : POPG : Chol and POPC : Chol lipids mix (18 μm and 12 μm, respectively) (Fig. 2(b) and Fig. S7, ESI†). We also observed some oblong-shaped GUVs with increased membrane elasticity in addition to perfect spherical GUVs (Fig. S13b and c, ESI†). We attribute this to the presence of the zinc cation during the GUV electroformation process. The cellular membrane curvature depends on lipid composition, influence of integral and peripheral membrane proteins, and cytoskeletal modifications.[41] Other than lipid composition our liposome models do not contain other structural influences. In the literature low concentration of ions such as La^{3+} and Gd^{3+} are reported to affect membrane curvature and induce shape changes in DOPC GUVs. We suspect free Zn^{2+} ions are acting in the same way. Since the cations cannot pass through the lipid bilayer, they induce lateral compression pressure on the exterior of the lipid membrane that causes a decrease in the surface area of the external monolayer while the area of the internal lipid layer remains the same. Such differences in the area between membranes of a bilayer cause reversible change in the shape of the vesicle for the duration that the ions are present in the proximity of the liposome.[42] We also observe degradation of MOF-177 over the course of 12 hours in aqueous environments, which is consistent with existing literature.[43] To confirm this, inductively coupled plasma optical emission spectroscopy (ICP OES) analysis was conducted on samples of the supernatant collected from the GUV@MOF-177 solutions over a 12 hour period. As expected, an increase in the concentration of Zn^{2+} ions was observed, and details included in ESI† (Fig. S32 and S33). Moreover, the brightfield images of MOF-177 particles observed for 12 hours, also show a notable reduction in the size of MOF particles though complete dissolution was not recorded (S34, ESI†).

We also tested two alkaline earth metal-containing MOFs. CaBDC only anchored to a negatively charged lipid mixture (Supplementary Video SV10, ESI†) and MgMOF-74 did not show any GUV anchoring and produced the smallest GUVs among all the MOFs in this study (Fig. S3–S5, ESI†). Research has shown that calcium ions have a greater tendency to bind negatively charged lipids in membranes than zwitterionic lipids.[44,45] As such, some GUVs were seen anchored to CaBDC in POPC : POPG : Chol lipid mixture despite of low electron affinity of calcium (Fig. 1(j) and Fig. S3, ESI†). Calcium MOFs are known for high hydrolytic stability because of strong coordination bonding.[46] The robust structural integrity results in the absence of solvated calcium ions that could potentially interfere with GUV swelling. GUVs were successfully produced in the presence of CaBDC with both POPC : Chol and DOPC lipid mixtures but the observed vesicle diameter was reduced (Fig. 2(a) and (b)). As noted, there was no observed GUV@MOF anchoring to MgMOF-74, and it showed the lowest yield of GUV formation along with the smallest diameter of GUVs formed. A possible reason is that MgMOF-74 is unstable under humid conditions, suggesting that it would be very unstable in the aqueous electroformation environment. This is because of the weak coordination bond between magnesium ions and oxygen atoms that dissociate the framework into its constituents releasing metal ions and organic molecules in the environment.[47] We have observed similar results on GUV formation with the zinc – dicarboxylic acid framework MOF-5,[48] which also decomposes in aqueous environments. Such MOFs will find important applications in drug delivery where short-term degradation of MOF is desired with the released metal ions such as magnesium and zinc being biocompatible.

GUV viability

The integrity of the GUV membrane, specifically in relation to their MOF anchoring capability, was investigated using POPC : POPG : Chol lipid mixture. This stability of immobilized GUV@-MOF was assessed at 2 and 6 hours when stored at room temperature, and over a 12 hour period when stored at 4 °C. Copper and zirconium based MOFs, with dicarboxylate ligands demonstrated remarkable GUV immobilization capacities, with anchored vesicles remaining intact when imaged after 2 hours (Fig. 5(d) and (h)), 6 hours (Fig. S14a and S18a, ESI†) and 12 hours (Fig. S14b and S18b, ESI†). Similar results were observed with tricarboxylate ligand MOFs HKUST-1 and MOF-808 after 2 hours (Fig. 5(e), (i)) and up to 12 hours (Fig. S15 and S19, ESI†). This extended stability is attributed to the excellent water stability of these MOFs, which prevents structural dissociation and ensures prolonged anchoring. The smaller particle size of the MIL-53 MOFs resulted in impotent GUV immobilization. While some GUVs anchored to MIL-53(Al) particles were stable for up to 2 hours (Fig. 5(a)), MIL-53(Fe) particles showed variable behaviour. We observed individual MIL-53(Fe) particles and clusters, with GUVs preferentially immobilized by the MOF clusters. The GUVs were anchored when imaged after 2 hours (Fig. 5(f)) and remained attached for up to 6 hours (Fig. S16a, ESI†),

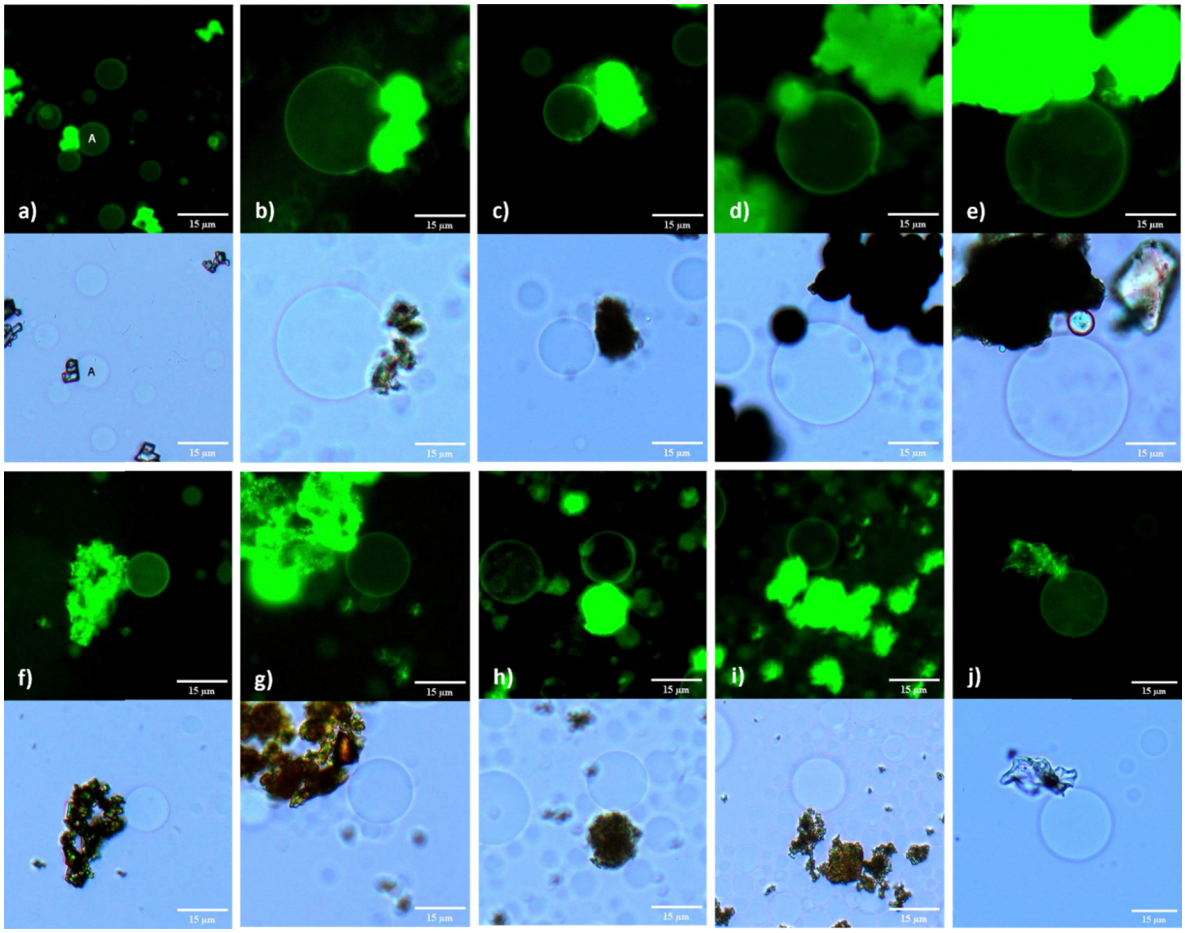

Fig. 5 Fluorescence and brightfield images of POPC : POPG : Chol (4 : 1 : 1) GUVs immobilized by MOF particles for 2 h (a) GUV A anchored to MIL-53(Al) (b) GUV/MIL-100(Al) (c) GUV/MOF-177 (d) GUV/CuBDC (e) GUV/HKUST-1 (f) GUV/MIL-53(Fe) (g) GUV/MIL-100(Fe) (h) GUV/UiO-66 (i) GUV/MOF-808 (j) GUV/CaBDC. Scale bars represent 15 μm.

while those associated with smaller MIL-53(Fe) particles displayed some mobility.

The extended metal node structure of MIL-100 MOFs likely contributed to their effective anchoring capacity in contrast to the MIL-53s. It seems that MOF structural features are important for GUV anchoring and its extended immobility. For the MIL-100(Al), the dispersion of MOF particles in the solution appeared to compromise GUV integrity. Aggregates of smaller vesicles were observed, many of which failed to fully separate (Fig. S12e, ESI†). GUVs did remain immobilized by the MOF particles when observed at the 2 hour (Fig. 5(b)) and 6 hour time mark (Fig. S12a, ESI†) and less over 12 hours (Fig. S12b, ESI†); however, unbound mobile GUVs exhibited significant changes in membrane curvature, losing their spherical shape within the 12 hour mark (Fig. S12d and e, ESI†). Conversely, MIL-100(Fe) particles provided efficient anchoring for GUVs, with consistent immobilization observed at the 2 hour (Fig. 5(g)), 6 hour (Fig. S17a, ESI†), and 12 hour (Fig. S17b, ESI†) intervals. Nevertheless, some vesicles began to exhibit signs of membrane instability by losing their spherical shape, suggesting that prolonged anchoring may induce stress on the vesicle membranes.

Biocompatible MOFs MOF-177 and CaBDC demonstrated the ability to immobilize GUVs formed with negatively charged lipid mixture at 2 hours (Fig. 5(c), (j)) and for a maximum duration of up to 6 hours (Fig. S13a and S20, ESI†). Although these MOFs exhibited limited stability, their ability to effectively anchor GUVs within this time frame is still noticeable. The capacity of these MOFs to interact with phospholipid membranes, even temporarily, suggests their usefulness in situations where short-term anchoring is required to facilitate the controlled release of therapeutics. These results underscore the promise of leveraging MOFs like CaBDC and MOF-177 in the development of advanced drug delivery platforms, where compatibility with biological system and effective membrane binding are crucial. An interesting finding of our study was the effect of MOFs on the viability of GUVs. In control experiments where GUVs were electroformed in the absence of MOFs, the vesicles remained viable for up to 4 days when stored at 4 °C. Whereas, in all cases where MOFs were included, GUVs gradually dissolved after 12 hours. This reduction in viability underscores the influence of MOFs on GUV stability, suggesting that while MOFs can effectively immobilize and interact with GUVs, they also effect membrane curvature and cause the degradation of the vesicles over time.

Summary of observed trends

Interestingly, we found that aluminium, copper (with POPC : POPG : Chol) and iron MOFs show increased GUV formation and anchoring with dicarboxylic acid ligand compared to the tricarboxylic acid ligands present in MIL-100(Al), HKUST-1, and MIL-100(Fe) (Fig. 2(a)). The binding of MOF particles to phospholipids is deemed to be an electrostatic or weakly coordinating interaction between cationic metal nodes (MOF node defects) and negatively charged phosphates. The number of anchored GUVs with aluminium and iron MIL-53 MOFs were 27 and 36, respectively and for MIL-100 MOFs were 24 and 34, respectively. There were instances of minimal anchoring with MIL-53(Fe) and MIL-53(Al), the values above are from different number of frames showing immobilized vesicles with each MOF category. We observed maximum anchoring of 48 GUVs immobilized by HKUST-1 compared to 20 GUVs with the other copper CuBDC MOF. The zirconium MOFs were recorded immobilizing 17 GUVs with UiO-66 and 20 GUVs with MOF-808. The MOFs with biofriendly metal centres displayed a varied trend with CaBDC immobilizing 25 GUVs, MOF-177 showing least anchoring capacity as only 9 GUVs were immobilized and MgMOF-74 did not immobilize any GUVs. In terms of lipid composition the POPC : POPG : Chol outperformed all lipid mixtures producing many MOF@GUV adducts. We noticed the size of anchored liposomes is indiscriminate of the type of MOF and lipid composition of the membrane.

The data indicate that each MOF interacts differently with the lipids, potentially influencing the assembly and stability of GUVs and thus altering the size distribution. This is a key observation, where we see a broad range of vesicle diameters with all lipids as expected from electroformation (Fig. 2(b) and 3). With the rise in temperature, the diameter of GUVs increases because of high fluidity and low bending modulus during GUV formation.[49] Electroformation for GUVs with DOPC : DPPC : Chol lipid mixture takes place at 45 °C, providing explanation to the observed larger size distribution (Fig. 3(c)). As noted above this temperature was required due to the higher T_m of DPPC. We noticed the mean vesicle diameters were larger than 20 μm with MIL-53(Al), MOF-177, Copper MOFs and zirconium MOFs compared to iron MOFs, CaBDC and MgMOF-74 when electroformed using DOPC : DPPC : Chol lipid mixture. The POPC : Chol lipid mixture demonstrated an overall narrow distribution in GUV sizes except for some GUVs in MIL-53(Al) (Fig. 3(b)).

While MOFs influence GUV immobilization and sizes, different MOFs also impact GUV yield. The frameworks MIL-MIL-100(Al), MIL-100(Fe), UiO-66, CaBDC and MgMOF-74 suppressed the number of GUVs produced compared to control in all lipid mixtures. The POPC : POPG : Chol lipid combination produces large number of GUVs with MOF-177 and CuBDC compared to other lipid mixtures in these MOFs and the control when no MOFs are included. MOF-808, particularly for the POPC : Chol lipid composition, demonstrated the highest vesicle yield among all MOFs, significantly surpassing the control. Moderate yields were observed for HKUST-1 and MIL-53(Fe) in all lipids suggesting the presence of these MOFs does not hinder vesicle swelling. In contrary, the POPC : Chol and DOPC : DPPC : Chol lipid mixture produced less than 20 GUVs with MIL-100(Al), MOF-177 and UiO-66 (Fig. 2(a)) demonstrating unsuitability of MOFs for potential applications. These observations collectively underscore the importance of MOF properties, such as particle size, surface area, and surface chemistry, in modulating different aspects of GUV formation.

Conclusion

MOFs have been extensively explored for their vast potential and remain at the cutting edge of research, with their deployment in the life sciences applications still on the horizon. The ability to immobilize GUVs using micron-sized MOF and GUV adducts without significantly compromising the structural integrity of the membrane is a standout aspect of this study, paving the way for prospective biomedical applications. We have adopted a straightforward and reproducible method to efficiently immobilize GUVs with aluminium, zinc, copper, iron, zirconium and calcium containing MOFs using saturated, unsaturated, and negatively charged lipid mixtures. The differences in immobilization efficiency are likely influenced by multiple factors. Based on the literature, MOFs electrostatically interact with the phosphate groups of lipids. Hence, MOFs with different metal centers may influence GUV immobilization due to differences in their coordination geometry. Additionally, we observed that larger MOF particles tended to anchor more GUVs compared to smaller particles, suggesting that MOF topology and surface area are also contributing factors. Larger particles may provide more binding sites for the GUVs or offer more favorable interactions due to their increased surface area.

The results revealed that CuBDC, HKUST-1, UiO-66, MOF-808, MIL-100(Al), and MIL-100(Fe) supported GUV formation and immobilization, which can be utilized in advanced bioimaging and tailored for advanced drug delivery applications. GUVs remained anchored to the zirconium and copper MOF surfaces for a remarkable period of 12 hours. The GUV yield in MIL-53 MOFs was comparatively higher than MIL-100 frameworks but the former showed fewer GUV immobilization. The biocompatible MOFs being susceptible to dissociation showed limited GUV formation, Zn-MOF-177 demonstrated minimal anchoring, CaBDC only anchored to GUVs formed with a negatively charged lipid mixture, yet GUVs remained bound for 6 hours. This feature is supportive for targeted therapeutic administration where short-term MOF–phospholipid interaction is required. Hence, this work shows the potential of MOFs as a versatile platform for biomaterials application in single liposome monitoring and assays, fluorescence-based data collection, and drug delivery.

Author contributions

AF: conceptualization, methodology, experimental, investigation, formal analysis, data curation, manuscript draft; MCL: experimental, data collection and analysis, writing; AGB: experimental; MVM: AFM analysis; BAB: funding procurement, conceptualization, writing.

Data availability

The raw data that underpins this work can be accessed through the University of New Brunswick data repository found here: **https://doi.org/10.25545/KBJHVD**.

Conflicts of interest

There are no conflicts to declare.

Acknowledgements

The authors respectfully acknowledge support for this work from the University of New Brunswick. B. A. B. is grateful for the support provided from the Natural Science and Engineering Council of Canada (RGPIN-2018-04021) as well as New Brunswick Foundation for Innovation (NBIF) Emerging Projects Program (EP-2020-005).

References

1 J. Yang and Y. Yang, *Small*, 2020, **16**, 1906846.
2 S. Keskin and S. Kızılel, *Ind. Eng. Chem. Res.*, 2011, **50**, 1799–1812.
3 N. Rabiee, M. Atarod, M. Tavakolizadeh, S. Asgari, M. Rezaei, O. Akhavan, A. Pourjavadi, M. Jouyandeh, E. C. Lima, A. Hamed Mashhadzadeh, A. Ehsani, S. Ahmadi and M. R. Saeb, *Microporous Mesoporous Mater.*, 2022, **335**, 111670.
4 N. Singh, S. Qutub and N. M. Khashab, *J. Mater. Chem. B*, 2021, **9**, 5925–5934.
5 F. Lyu, Y. Zhang, R. N. Zare, J. Ge and Z. Liu, *Nano Lett.*, 2014, **14**, 5761–5765.
6 Y. H. Wijesundara, F. C. Herbert, O. Trashi, I. Trashi, O. R. Brohlin, S. Kumari, T. Howlett, C. E. Benjamin, A. Shahrivarkevishahi, S. D. Diwakara, S. D. Perera, S. A. Cornelius, J. P. Vizuet, K. J. Balkus, R. A. Smaldone, N. J. De Nisco and J. J. Gassensmith, *Chem. Sci.*, 2022, **13**, 13803–13814.
7 L. Du, W. Chen, P. Zhu, Y. Tian, Y. Chen and C. Wu, *Biotechnol. J.*, 2021, **16**, 1900424.
8 Z. Li, Y. Ding, X. Wu, J. Ge, P. Ouyang and Z. Liu, *RSC Adv.*, 2016, **6**, 20772–20776.
9 S. F. Fenz and K. Sengupta, *Integr. Biol.*, 2012, **4**, 982–995.
10 H. Pick, A. C. Alves and H. Vogel, *Chem. Rev.*, 2018, **118**, 8598–8654.
11 A. Karami, A. Ahmed, R. Sabouni, G. A. Husseini, M. Al Sharabati, N. AlSawaftah and V. Paul, *Colloids Surf., B*, 2022, 112599.
12 X. Li, G. Salzano, J. Qiu, M. Menard, K. Berg, T. Theodossiou, C. Ladavière and R. Gref, *Front. Bioeng. Biotechnol.*, 2020, **8**, 1027.
13 F. C. Herbert, S. S. Abeyrathna, N. S. Abeyrathna, Y. H. Wijesundara, O. R. Brohlin, F. Carraro, H. Amenitsch, P. Falcaro, M. A. Luzuriaga, A. Durand-Silva, S. D. Diwakara, R. A. Smaldone, G. Meloni and J. J. Gassensmith, *Nat. Commun.*, 2021, **12**, 2202.
14 S. Kumari, Y. H. Wijesundara, T. S. Howlett, F. C. Herbert, A. Raja, I. Trashi, J. Gadhvi, N. J. De Nisco and J. Gassensmith, Biolistic Delivery of MOF-Protected Liposomes, Chemistry, 2022.
15 H. Hu, Z. Wang, L. Cao, L. Zeng, C. Zhang, W. Lin and C. Wang, *Nat. Chem.*, 2021, **13**, 358–366.
16 S. Wang, W. Morris, Y. Liu, C. M. McGuirk, Y. Zhou, J. T. Hupp, O. K. Farha and C. A. Mirkin, *Angew. Chem., Int. Ed.*, 2015, **54**, 14738–14742.
17 E. Ploetz, A. Zimpel, V. A. Cauda, D. Bauer, D. C. Lamb, C. Haisch, S. Zahler, A. M. Vollmar, S. Wuttke, S. Wuttke and H. Engelke, *Adv. Mater.*, 2020, **32**, 1907267.
18 A. Moga, N. Yandrapalli, R. Dimova and T. Robinson, *ChemBioChem*, 2019, **20**, 2674–2682.
19 X. Wang, L. Tian, H. Du, M. Li, W. Mu, B. W. Drinkwater, X. Han and S. Mann, *Chem. Sci.*, 2019, **10**, 9446–9453.
20 P. Kuhn, K. Eyer, T. Robinson, F. I. Schmidt, J. Mercer and P. S. Dittrich, *Integr. Biol.*, 2012, **4**, 1550.
21 B. Van Lengerich, R. J. Rawle and S. G. Boxer, *Langmuir*, 2010, **26**, 8666–8672.
22 Q. Li, S. Li, X. Zhang, W. Xu and X. Han, *Nat. Commun.*, 2020, **11**, 232.
23 J. Korlach, C. Reichle, T. Müller, T. Schnelle and W. W. Webb, *Biophys. J.*, 2005, **89**, 554–562.
24 R. B. Lira, J. Steinkühler, R. L. Knorr, R. Dimova and K. A. Riske, *Sci. Rep.*, 2016, **6**, 25254.
25 I. Kusters, N. Mukherjee, M. R. De Jong, S. Tans, A. Koçer and A. J. M. Driessen, *PLoS One*, 2011, **6**, e20435.
26 K. S. Horger, D. J. Estes, R. Capone and M. Mayer, *J. Am. Chem. Soc.*, 2009, **131**, 1810–1819.
27 Y. Kazayama, T. Teshima, T. Osaki, S. Takeuchi and T. Toyota, *Anal. Chem.*, 2016, **88**, 1111–1116.
28 A. Yamada, S. Lee, P. Bassereau and C. N. Baroud, *Soft Matter*, 2014, **10**, 5878.
29 C. S. Jennings, J. S. Rossman, B. A. Hourihan, R. J. Marshall, R. S. Forgan and B. A. Blight, *Soft Matter*, 2021, **17**, 2024–2027.
30 C. Prévost, H. Zhao, J. Manzi, E. Lemichez, P. Lappalainen, A. Callan-Jones and P. Bassereau, *Nat. Commun.*, 2015, **6**, 8529.
31 A. Dickey and R. Faller, *Biophys. J.*, 2008, **95**, 2636–2646.
32 E. Moumen, L. Bazzi and S. El Hankari, *Process Saf. Environ. Prot.*, 2022, **160**, 502–512.
33 K. G. K. Vargas, Z. Qi and V. Quezada-Novoa, *J. Environ. Chem. Eng.*, 2021, **9**, 106849.
34 I. A. Kumar, A. Jeyaseelan, S. Ansar and N. Viswanathan, *J. Environ. Chem. Eng.*, 2022, **10**, 107233.
35 D. N. Lee, Y. R. Kim, Y. Kim, B. J. Park, S. J. Lee, S.-J. Kim and J. H. Shin, *ACS Appl. Bio Mater.*, 2022, **5**, 4301–4309.
36 J. Yang, X. Chen, Y. Li, Q. Zhuang, P. Liu and J. Gu, *Chem. Mater.*, 2017, **29**, 4580–4589.
37 Y. Bai, Y. Dou, L.-H. Xie, W. Rutledge, J.-R. Li and H.-C. Zhou, *Chem. Soc. Rev.*, 2016, **45**, 2327–2367.
38 A. Pattammattel, I. K. Deshapriya, R. Chowdhury and C. V. Kumar, *Langmuir*, 2013, **29**, 2971–2981.
39 X. Zhu, J. Gu, Y. Wang, B. Li, Y. Li, W. Zhao and J. Shi, *Chem. Commun.*, 2014, **50**, 8779–8782.
40 M. Moharramnejad, A. Ehsani, S. Salmani, M. Shahi, R. E. Malekshah, Z. S. Robatjazi and H. Parsimehr, *J. Inorg. Organomet. Polym.*, 2022, **32**, 3339–3354.

41 H. T. McMahon and J. L. Gallop, *Nature*, 2005, **438**, 590–596.
42 T. Tanaka, Y. Tamba, S. M. Masum, Y. Yamashita and M. Yamazaki, *Biochim. Biophys. Acta, Biomembr.*, 2002, **1564**, 173–182.
43 D. Saha and S. Deng, *J. Phys. Chem. Lett.*, 2010, **1**, 73–78.
44 J. Diao, T.-Y. Yoon, Z. Su, Y.-K. Shin and T. Ha, *Langmuir*, 2009, **25**, 7177–7180.
45 B. Luan, K. L. Chen and R. Zhou, *J. Phys. Chem. Lett.*, 2016, **7**, 2434–2438.
46 F. F. Sukatis, S. Y. Wee and A. Z. Aris, *Water Res.*, 2022, **218**, 118406.
47 S. Zuluaga, E. M. A. Fuentes-Fernandez, K. Tan, F. Xu, J. Li, Y. J. Chabal and T. Thonhauser, *J. Mater. Chem. A*, 2016, **4**, 5176–5183.
48 Y. Ming, J. Purewal, J. Yang, C. Xu, R. Soltis, J. Warner, M. Veenstra, M. Gaab, U. Müller and D. J. Siegel, *Langmuir*, 2015, **31**, 4988–4995.
49 T. Shimanouchi, H. Umakoshi and R. Kuboi, *Langmuir*, 2009, **25**, 4835–4840.

